



**HAL**  
open science

## Discovery of a Neutral 40-Pd II -Oxo Molecular Disk, [Pd 40 O 24 (OH) 16 (CH 3 ) 2 AsO 2 16 ]: Synthesis, Structural Characterization, and Catalytic Studies

Saurav Bhattacharya, Xiang Ma, Ali S Mougharbel, Mohamed Haouas, Pei Su, Michael Forrester F J Espenship, Dereje H Taffa, Helge Jaensch, Anton-Jan Bons, Tobias Stuerzer, et al.

### ► To cite this version:

Saurav Bhattacharya, Xiang Ma, Ali S Mougharbel, Mohamed Haouas, Pei Su, et al.. Discovery of a Neutral 40-Pd II -Oxo Molecular Disk, [Pd 40 O 24 (OH) 16 (CH 3 ) 2 AsO 2 16 ]: Synthesis, Structural Characterization, and Catalytic Studies. *Inorganic Chemistry*, 2021, 60 (22), pp.17339-17347. 10.1021/acs.inorgchem.1c02749 . hal-03476436

**HAL Id: hal-03476436**

**<https://hal.science/hal-03476436>**

Submitted on 12 Dec 2021

**HAL** is a multi-disciplinary open access archive for the deposit and dissemination of scientific research documents, whether they are published or not. The documents may come from teaching and research institutions in France or abroad, or from public or private research centers.

L'archive ouverte pluridisciplinaire **HAL**, est destinée au dépôt et à la diffusion de documents scientifiques de niveau recherche, publiés ou non, émanant des établissements d'enseignement et de recherche français ou étrangers, des laboratoires publics ou privés.

# Discovery of a Neutral 40-Pd<sup>II</sup>-Oxo Molecular Disk, [Pd<sub>40</sub>O<sub>24</sub>(OH)<sub>16</sub>{(CH<sub>3</sub>)<sub>2</sub>AsO<sub>2</sub>}<sub>16</sub>]: Synthesis, Structural Characterization and Catalytic Studies

Saurav Bhattacharya,<sup>[a]</sup> Xiang Ma,<sup>[a]</sup> Ali S. Mougharbel,<sup>[a]</sup> Mohamed Haouas,<sup>[b]</sup> Pei Su,<sup>[c]</sup> Michael Forrester Espenship,<sup>[c]</sup> Dereje H. Taffa,<sup>[d]</sup> Helge Jaensch,<sup>[e]</sup> Anton-Jan Bons,<sup>[e]</sup> Tobias Stuerzer,<sup>[f]</sup> Michael Wark,<sup>[d]</sup> Julia Laskin,<sup>[c]</sup> Emmanuel Cadot,<sup>[b]</sup> and Ulrich Kortz\*<sup>[a]</sup>

[a] Dr. S. Bhattacharya, X. Ma, Dr. A. S. Mougharbel, Prof. U. Kortz  
Department of Life Sciences and Chemistry  
Jacobs University  
Campus Ring 1, 28759 Bremen, Germany  
E-mail: [u.kortz@jacobs-university.de](mailto:u.kortz@jacobs-university.de)

[b] Dr. M. Haouas, Prof. E. Cadot  
Institut Lavoisier de Versailles, CNRS, UVSQ  
Université Paris-Saclay, Versailles, France

[c] P. Su, M. F. Espenship, Prof. J. Laskin  
Department of Chemistry  
Purdue University  
560 Oval Drive, West Lafayette, Indiana 47907, United States

[d] Dr. D. H. Taffa, Prof. M. Wark  
Institute of Chemistry  
Carl von Ossietzky University Oldenburg  
26129 Oldenburg, Germany

[e] Dr. H. Jaensch, Dr. A.-J. Bons  
Global Chemical Research  
ExxonMobil Chemical Europe Inc.  
1831 Machelen, Belgium

[f] Dr. Tobias Stuerzer  
Bruker AXS GmbH  
Oestliche Rheinbrueckenstr. 49  
76187 Karlsruhe, Germany

---

**ABSTRACT:** We report on the synthesis and structural characterization of the giant discrete and neutral molecular disk, [Pd<sub>40</sub>O<sub>24</sub>(OH)<sub>16</sub>{(CH<sub>3</sub>)<sub>2</sub>AsO<sub>2</sub>}<sub>16</sub>] (**Pd<sub>40</sub>**), comprising a 40-palladium-oxo core that is capped by 16 dimethylarsinate moieties, resulting in a palladium-oxo cluster (POC) with a diameter of ~2 nm. **Pd<sub>40</sub>**, which is the largest neutral Pd-based oxo-cluster, can be isolated either as a discrete species or constituting a 3D H-bonded organic-inorganic framework (HOIF) with a 12-tungstate Keggin ion [SiW<sub>12</sub>O<sub>40</sub>]<sup>4-</sup> or [GeW<sub>12</sub>O<sub>40</sub>]<sup>4-</sup>. <sup>1</sup>H and <sup>13</sup>C NMR as well as 1H-DOSY NMR studies indicate that **Pd<sub>40</sub>** is stable in aqueous solution, which is also confirmed by ESI-MS studies. **Pd<sub>40</sub>** was also immobilized on a mesoporous support (SBA15) followed by the generation of size-controlled Pd-nanoparticles (diameter ~2-6 nm, as based on HR-TEM), leading to an effective heterogeneous hydrogenation catalyst for the transformation of various arenes to saturated carbocycles.

---

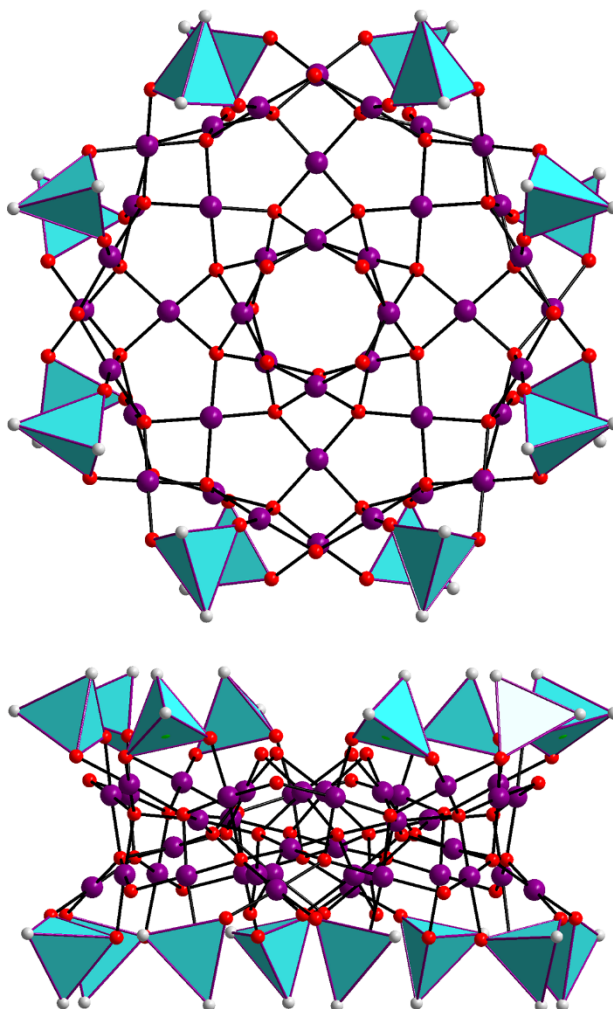
## INTRODUCTION

Discrete metal-oxo clusters, a subset of inorganic coordination cage complexes, are comprised of metal ions which are bridged by various oxygen-based ligands, such as  $O^{2-}$ ,  $OH^-$  or  $H_2O$ , leading to molecular entities with well-defined formulae and structures. The shape, size and composition of such metal-oxo clusters can at times be designed by exerting control over the degree of hydrolysis and condensation,<sup>1</sup> e.g. by subtly manipulating the various reaction parameters, such as concentration and type of metal ions, temperature, pH, ionic strength, redox environment, and the choice of capping ligands that arrest the aggregation process of the metal-oxo clusters, thereby preventing the formation of amorphous and insoluble products. Extensive research in this field has led to the discovery of several transition metal- and lanthanide-based metal-oxo/hydroxo clusters,<sup>2</sup> which have shown immense promise as functional materials for single-molecular magnetism,<sup>3</sup> cryogenic magnetic cooling devices,<sup>4</sup> photocatalytic water oxidation,<sup>5</sup> and band-gap tuning.<sup>6</sup> In addition, the supramolecular structuring and organization of these metal-oxo clusters have led to the realization of either metal-organic frameworks (MOFs),<sup>7</sup> or all-inorganic open-framework materials,<sup>8</sup> by the judicious choice of organic and inorganic ligands, respectively, that connect the metal-oxo clusters (secondary building units, SBUs) in three dimensions. These assemblies have shown to be useful materials for gas-separation as well as heterogeneous electro- or photocatalysis.<sup>7,8</sup>

Polyoxometalates (POMs), a prominent subclass of discrete metal-oxo clusters, are polynuclear anions that are formed by connecting early *d*-block metal ions in high oxidation states, such as  $V^V$ ,  $Mo^VI$ , and  $W^VI$ , with oxo ligands, and such species exhibit a diverse range of shapes, sizes and compositions.<sup>9</sup> POMs exhibit high redox, thermal and electro-/photochemical stability and consequently find use as materials for catalysis, magnetism and molecular electronics.<sup>10</sup> In addition, POMs can be covalently or electrostatically linked with other cationic polynuclear complexes, leading to composite assemblies.<sup>11</sup>

Döbereiner's proposition that structurally precise noble metal-based oxo-clusters could serve as models to comprehend the molecular mechanism of noble metal-based catalysis have inspired researchers over the years to isolate POMs with noble metals as addenda atoms.<sup>12</sup> The breakthrough in 2004 by Wickleder's group with the discovery of the first polyoxo-12-platinate(III),  $[Pt^{III}_{12}O_8(SO_4)_{12}]^{4-}$  was followed by the discovery of the first polyoxopalladate(II) (POP),  $[Pd^{II}_{13}As_8O_{34}(OH)_6]^{8-}$  and the first polyoxoaurate(III),  $[Au^{III}_4As_4O_{20}]^{8-}$  by Kortz's group in 2008 and 2010, respectively,<sup>13a-c</sup> which eventually prompted the discovery of a plethora of composition, shape and size-tuned noble metal ion-based POMs.<sup>13-16</sup> In addition to  $Pt^{III}$ ,  $Pd^{II}$  and  $Au^{III}$ , other noble metal ion-derived metal-oxo clusters have also been isolated, most of which are either anionic or cationic.<sup>17</sup> Neutral metal oxo/hydroxo-clusters derived from  $Ti^{IV}$ ,  $Zr^{IV}$  and  $Al^{III}$  utilizing bidentate carboxylate capping groups are common, but there is only a small number of corresponding noble metal-based variants.<sup>2b-g,18</sup> Very recently, we reported the first discrete and neutral ring-shaped palladium(II)-oxo clusters,  $[Pd_{16}O_8(OH)_8((CH_3)_2AsO_2)_8]$  (**Pd<sub>16</sub>**),  $[Pd_{16}O_8(OH)_5Cl_3((CH_3)_2AsO_2)_8]$  (**Pd<sub>16</sub>Cl**) and  $[Pd_{24}O_{12}(OH)_8((CH_3)_2AsO_2)_{16}]$  (**Pd<sub>24</sub>**).<sup>19</sup>

Metal-oxo clusters can be considered as pre-nucleated metal nanoclusters which, when distributed uniformly on a support



followed by reduction, would lead to metal nanoparticles having controlled sizes that would be largely dependent on the size of the parent metal-oxo cluster. This concept was demonstrated recently by utilizing various anionic POPs as model metal-oxo clusters<sup>14b</sup> and allows for improved size-control of the metal-nanoparticles, which is typically difficult to achieve using conventional methods, such as organic ligands, ionic liquids or dendrimer-stabilized metal nanoparticles.<sup>20</sup> Here we report on the synthesis, structural and physicochemical characterization of a large, discrete and neutral disk-shaped palladium(II)-oxo cluster (POC) and its utilization as a heterogeneous catalyst.

## RESULTS AND DISCUSSION

### Synthesis and structure.

The neutral disk-shaped 40-palladium(II)-oxo cluster,  $[Pd_{40}O_{24}(OH)_{16}\{(CH_3)_2AsO_2\}_{16}]$  (**Pd<sub>40</sub>**, see Figure 1), was synthesized by stirring a mixture of palladium(II) acetate and barium(II) nitrate in a sodium dimethylarsinate ( $(CH_3)_2AsO_2Na$ , also known as sodium cacodylate, Na-cac) buffer solution at pH 6.5 for 14 hours at room temperature followed by pH adjustment to  $\sim 7.5$  by addition of aq. NaOH solution and stirring the resulting deep-red solution at room temperature for 10 hours more before filtering. A dark-brown precipitate was obtained after 1-2 months, which was recrystallized from deionized water to obtain dark-red, plate-shaped crystals of

$[\text{Pd}_{40}\text{O}_{24}(\text{OH})_{16}\{(\text{CH}_3)_2\text{AsO}_2\}_{16}] \cdot 5\text{Ba}(\text{NO}_3)_2 \cdot 7\{\text{Na}(\text{CH}_3)_2\text{AsO}_2\} \cdot 2\text{NaCH}_3\text{COO} \cdot \text{NaNO}_3 \cdot 80\text{H}_2\text{O}$  (**Pd<sub>40</sub>-Ba**), for details see Experimental Section in the ESI. Alternatively, **Pd<sub>40</sub>** could be synthesized and isolated in a different form by stirring a mixture of palladium(II) acetate and  $\text{Na}_{10}[\alpha\text{-XW}_9\text{O}_{34}]$  (X = Si, Ge) in a cacodylate buffer solution at pH 7 for 2 days at room temperature, followed by pH adjustment to ~8 by addition of aq. NaOH solution and stirring the resulting deep-red solution at room temperature for a day more before filtering. Deep-red, cube-shaped crystals of  $\text{Na}_{14}[\text{Pd}_{40}\text{O}_{32}(\text{OH})_8\{(\text{CH}_3)_2\text{AsO}_2\}_{16}(\text{SiW}_{12}\text{O}_{40})_{1.5}] \cdot 2\{\text{Na}(\text{CH}_3)_2\text{AsO}_2\} \cdot 2\{\text{Na}(\text{CH}_3\text{COO})\} \cdot 135\text{H}_2\text{O}$  (**Pd<sub>40</sub>-SiW<sub>12</sub>**) or  $\text{Na}_{10}[\text{Pd}_{40}\text{O}_{24}(\text{OH})_{16}\{(\text{CH}_3)_2\text{AsO}_2\}_{16}(\text{GeW}_{12}\text{O}_{40})_{2.5}] \cdot 4\{\text{Na}(\text{CH}_3)_2\text{AsO}_2\} \cdot 110\text{H}_2\text{O}$  (**Pd<sub>40</sub>-GeW<sub>12</sub>**) were obtained within a week in significantly higher yields (29% and 20%, respectively) as compared to **Pd<sub>40</sub>-Ba** (5%), for details see Experimental Section in the ESI. Using the plenary Keggin ion  $[\text{XW}_{12}\text{O}_{40}]^{4-}$  (X = Si, Ge) as a reagent instead of the trilacunary derivative surprisingly led to lower yields. Single-crystal X-ray structural analysis on **Pd<sub>40</sub>-Ba**, **Pd<sub>40</sub>-SiW<sub>12</sub>**, and **Pd<sub>40</sub>-GeW<sub>12</sub>**, respectively, indicated that the same neutral molecular disk **Pd<sub>40</sub>** is present in all three compounds. **Pd<sub>40</sub>** comprises 40 square-planar coordinated palladium(II) ions and the structure can be visualized as a central square-antiprismatic  $[\text{Pd}_8\text{O}_8(\text{OH})_8]^{8-}$  unit, which is surrounded by a cyclic  $[\text{Pd}_8\text{O}_{16}]^{16-}$  unit. This, in turn, is further encircled by a  $[\text{Pd}_{24}(\text{OH})_8((\text{CH}_3)_2\text{As})_{16}]^{24+}$  unit, leading to the overall neutral **Pd<sub>40</sub>** unit (Figures 1 and S1). Alternatively, **Pd<sub>40</sub>** can be seen as being composed of a  $[\text{Pd}_{16}\text{O}_{16}(\text{OH})_8]^{8-}$  (**Pd<sub>16</sub>**) unit,<sup>19</sup> which is further encircled by 24  $\text{Pd}^{2+}$  ions and 16 cacodylate capping groups. Thus, **Pd<sub>40</sub>** can be considered as an extended version of **Pd<sub>16</sub>**. The higher nuclearity of **Pd<sub>40</sub>** can be correlated with the higher reaction pH (~7.5 – 8) as compared to the reaction pH of ~5.7 – 7 for **Pd<sub>16</sub>** and **Pd<sub>24</sub>**, respectively. The discrete **Pd<sub>40</sub>** has an idealized point group symmetry of  $D_{4d}$  with the  $C_4$  principal axis of rotation passing through the central square-antiprismatic unit. **Pd<sub>40</sub>** crystallizes either in the monoclinic space group  $C2/c$  when associated with  $\text{Ba}^{2+}$  ions (**Pd<sub>40</sub>-Ba**) or in the cubic space group  $\text{Im-}3\text{m}$  when associated with either the  $[\text{SiW}_{12}\text{O}_{40}]^{4-}$  (**Pd<sub>40</sub>-SiW<sub>12</sub>**) or the  $[\text{GeW}_{12}\text{O}_{40}]^{4-}$  (**Pd<sub>40</sub>-GeW<sub>12</sub>**) Keggin ions in the solid state (Table S1). Typical Pd-O bond distances and O-Pd-O bond angles are listed in Tables S2-S5, all indicating a typical square-planar coordination geometry for the  $\text{Pd}^{2+}$  centers. Bond valence sum (BVS) calculations on the central and peripheral  $\mu_2\text{-O}$  groups yield values of 0.97 – 1.10 (Tables S6, S7), suggesting the presence of a single negative charge on the  $\mu_2\text{-O}$  groups, which could either be charge-compensated by a covalently linked proton ( $\mu_2\text{-OH}$  groups) or by an electrostatically attracted counter cation ( $\text{Ba}^{2+}$ ,  $\text{Na}^+$ ). Elemental analysis for **Pd<sub>40</sub>-Ba** indicated the presence of exclusively  $\mu_2\text{-OH}$  groups, suggesting only a weak interaction with the  $\text{Ba}^{2+}$  ions surrounding **Pd<sub>40</sub>** (Figure S2). However, from the elemental analysis results for **Pd<sub>40</sub>-SiW<sub>12</sub>** we observed that the eight  $\mu_2\text{-O}$  groups in the central core of **Pd<sub>40</sub>** are deprotonated and associated with eight  $\text{Na}^+$  ions, which could not be identified by single-crystal XRD studies due to crystallographic disorder. However, in solution, the eight deprotonated  $\mu_2\text{-O}$  groups re-protonate to yield the neutral **Pd<sub>40</sub>** as observed from ESI-MS studies (*vide infra*). The eight peripheral  $\mu_2\text{-OH}$  groups (O5 and O9) of the **Pd<sub>40</sub>** unit in **Pd<sub>40</sub>-SiW<sub>12</sub>** are strongly H-bonded to the terminal oxo groups of the  $[\text{SiW}_{12}\text{O}_{40}]^{4-}$  units (O16 and O20), see Figures S3 and S6. There are two crystallographically independent  $[\text{SiW}_{12}\text{O}_{40}]^{4-}$  Keggin ions per

formula unit: one of these is fully occupied, whereas the other has an occupancy of 0.5 (Figure S4). Each fully occupied  $[\text{SiW}_{12}\text{O}_{40}]^{4-}$  ion is H-bonded to four **Pd<sub>40</sub>** in a tetrahedral fashion (Figure S5) that leads to a perpendicularly-oriented octahedral arrangement with the equatorial positions occupied by the Keggin ions, whereas the axial positions are occupied by **Pd<sub>40</sub>** (Figure S6). The formation of the plenary Keggin ion at pH 7-8 is highly unusual and most likely driven by H-bonding interactions with **Pd<sub>40</sub>** and the resulting highly-symmetrical supramolecular arrangement. The octahedral units are further linked in 3D space *via* H-bonding interactions to form a supramolecular 3D hydrogen-bonded organic-inorganic framework (HOIF), consisting of cylindrical channels that run in all three crystallographic directions (Figure S6). These channels are occupied by the half-occupied Keggin ions (held in space *via* H-bonding interactions) as well as  $\text{Na}^+$  ions, cacodylates, acetates and lattice water molecules (Figure S7). If we consider each of the octahedral arrangements as a secondary building unit (SBU), then each of the SBUs is connected to four other SBUs through the equatorial Keggin unit, leading to a four-connected *nbo* network topology having the Schläfli symbol  $6^4.8^2$  (Figure S8). This is only the second example of noble metal-oxo-cluster-based HOIFs, the first being reported recently by our group.<sup>19</sup> The innate difficulty of controlling the extent of H-bonding interactions between inorganic and organic molecular components is the reason that such types of frameworks are rare.<sup>21</sup> The formation of the 3D HOIF in **Pd<sub>40</sub>-SiW<sub>12</sub>** is the driving force towards a faster crystallization and a much higher yield (29%) as compared to **Pd<sub>40</sub>-Ba** (5%). The framework stability of **Pd<sub>40</sub>-SiW<sub>12</sub>** was further confirmed by powder XRD (PXRD) studies, which showed that the PXRD patterns of the as-prepared **Pd<sub>40</sub>-SiW<sub>12</sub>** and its dehydrated and rehydrated forms matched well with the PXRD pattern simulated from single-crystal XRD data (Figure S9a). We observed only a moderate loss of crystallinity upon dehydration and subsequent rehydration, where dehydration was achieved by heating the compound at 50 °C for 1 h under vacuum and rehydration was achieved by keeping the dehydrated sample in an atmosphere of water vapour at room temperature. This behaviour was also demonstrated by thermogravimetric analysis (TGA) on **Pd<sub>40</sub>-SiW<sub>12</sub>** (Figure S9b). Thus, we see that the introduction of the  $[\text{SiW}_{12}\text{O}_{40}]^{4-}$  Keggin moiety as a H-bond acceptor introduces a certain degree of stability and crystallinity to the compound *via* the formation of a supramolecular solid-state assembly. The unit cell parameters for single crystals of **Pd<sub>40</sub>-GeW<sub>12</sub>** were similar to those of **Pd<sub>40</sub>-SiW<sub>12</sub>** (footnote of Table S1). However, we were not able to collect proper single-crystal XRD data for **Pd<sub>40</sub>-GeW<sub>12</sub>** because the crystals consistently formed in very small sizes and the diffraction quality was

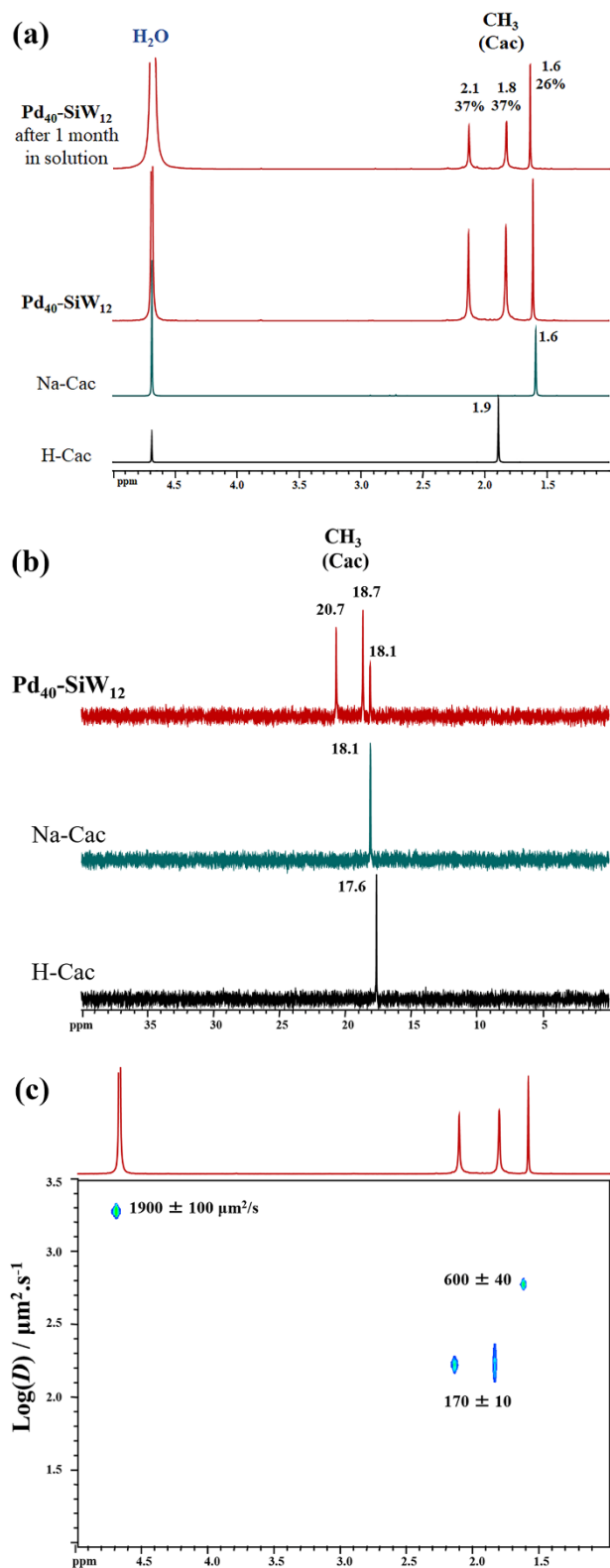


**Figure 2.** Solution  $^1\text{H}$  (a) and  $^{13}\text{C}$  (b) NMR spectra of  $\text{Pd}_{40}\text{-SiW}_{12}$  in  $\text{D}_2\text{O}$  compared with the spectra of cacodylic acid (H-cac) and sodium cacodylate (Na-cac) as references. (c)  $^1\text{H}$ -DOSY NMR spectrum of  $\text{Pd}_{40}\text{-SiW}_{12}$  in  $\text{D}_2\text{O}$ . See text for details. The NMR signal at ca. 4.7 ppm with  $D = 1900 \mu\text{m}^2/\text{s}$  corresponds to water molecules.

poor. However, the TGA curves, IR spectra (Experimental Section in the ESI, Figures S10 and S11) and the solution-state

NMR spectra (*vide infra*) for  $\text{Pd}_{40}\text{-SiW}_{12}$  and  $\text{Pd}_{40}\text{-GeW}_{12}$  were found to be very similar, suggesting that they are isostructural.

### Solution, and DOSY NMR spectroscopy.

In order to investigate the solution stability of  $\text{Pd}_{40}$ , we decided to measure  $^1\text{H}$  and  $^{13}\text{C}$  NMR. As  $\text{Pd}_{40}$  is present in all three compounds  $\text{Pd}_{40}\text{-Ba}$ ,  $\text{Pd}_{40}\text{-GeW}_{12}$ , and  $\text{Pd}_{40}\text{-SiW}_{12}$ , we decided to mainly focus on  $\text{Pd}_{40}\text{-SiW}_{12}$ , as it has the highest yield. The solution  $^1\text{H}$  NMR spectra in  $\text{D}_2\text{O}$  of the references H-cac and Na-cac resulted in sharp peaks at 1.9 and 1.6 ppm, respectively, which correspond to the protons of the two equivalent methyl groups coordinated to the  $\text{As}^{\text{V}}$  atom (Figure 2a). The  $^1\text{H}$  NMR spectrum of  $\text{Pd}_{40}\text{-SiW}_{12}$  in  $\text{D}_2\text{O}$  exhibits three distinct peaks at 1.6, 1.8 and 2.1 ppm, respectively. The peak at 1.6 ppm corresponds to the methyl protons of free cocrystallized cacodylate ion, and the peaks at 1.8 and 2.1 ppm (1:1 ratio) correspond to the hydrogens of the two cacodylate methyl groups in  $\text{Pd}_{40}$ . Although all cacodylates in  $\text{Pd}_{40}$  are structurally equivalent, the two methyl groups are not. A careful inspection of the  $\text{Pd}_{40}$  structure (Figure 1) reveals that one of them points towards the  $\text{Pd}_{40}\text{-oxo}$  core and the other away from it, resulting in structural and hence magnetic inequivalence. This was further corroborated by  $^{13}\text{C}$  solution NMR studies. Cacodylic acid (H-cac) and sodium cacodylate (Na-cac), exhibited sharp singlets at 17.6 and 18.1 ppm, respectively, which correspond to the two methyl carbons coordinated to the arsenic atom (Figure 2b). On the other hand, the  $^{13}\text{C}$  NMR spectrum of  $\text{Pd}_{40}\text{-SiW}_{12}$  exhibits three distinct sharp peaks (in analogy to its  $^1\text{H}$  NMR spectrum) at 18.1, 18.7 and 20.7 ppm corresponding to the methyl groups of free cocrystallized cacodylate ions and the two inequivalent methyl groups of cacodylate bound to  $\text{Pd}_{40}$ , respectively (Figure 2b). The stability of the discrete, molecular  $\text{Pd}_{40}$  in solution was further proven by measuring the  $^1\text{H}$  NMR spectrum of the same solution after a month, which showed that all the peaks remained intact and no new peaks that would indicate decomposition of the  $\text{Pd}_{40}$  appeared (see Figure 2a). The  $^1\text{H}$ -DOSY NMR spectrum of  $\text{Pd}_{40}\text{-SiW}_{12}$  (Figure 2c) confirms the assignments of the  $^1\text{H}$ -NMR spectrum showing that the signal corresponding to the free cacodylate at 1.6 ppm has a diffusion coefficient  $D$  of  $600 \mu\text{m}^2/\text{s}$ , whereas both the peaks at 1.8 and 2.1 ppm (corresponding to the two inequivalent cacodylate methyl groups on  $\text{Pd}_{40}$ ) are perfectly aligned and indicate the same diffusion coefficient  $D$  of  $170 \mu\text{m}^2/\text{s}$ , which should correspond to the diffusion rate of  $\text{Pd}_{40}$ . Such a large difference for the  $D$  values by a factor of 3 is indicative of the binding of the cacodylate ligands to a nanoscopic object such as  $\text{Pd}_{40}$ . The  $D$  value of  $600 \mu\text{m}^2/\text{s}$  for the peak at 1.6 ppm (free Na-cac) is smaller than the value of  $640 \mu\text{m}^2/\text{s}$  observed for Na-cac alone in solution (i.e. in the absence of any  $\text{Pd}_{40}$ ). This indicates that in solutions of  $\text{Pd}_{40}$  the dissociated cacs are in equilibrium with the coordinated cacs and the degree of dissociation has been found to be ca. 20% (from integrating  $^1\text{H}$  NMR spectra of Figure 2a). The ratio of dissociation/coordination has been found to remain unchanged even after keeping the solution for a month at room temperature. The solution  $^1\text{H}$  NMR spectra of  $\text{Pd}_{40}\text{-Ba}$  and  $\text{Pd}_{40}\text{-GeW}_{12}$  exhibit peaks fully consistent with what is observed for  $\text{Pd}_{40}\text{-SiW}_{12}$ , indicating that  $\text{Pd}_{40}$  is the same in all three compounds (Figure S12).

### Mass spectrometry.

The positive mode ESI-MS spectrum of  $\text{Pd}_{40}\text{-SiW}_{12}$  is shown in Figure 3a. In the  $m/z$  range of 2300-2800, all the peaks are

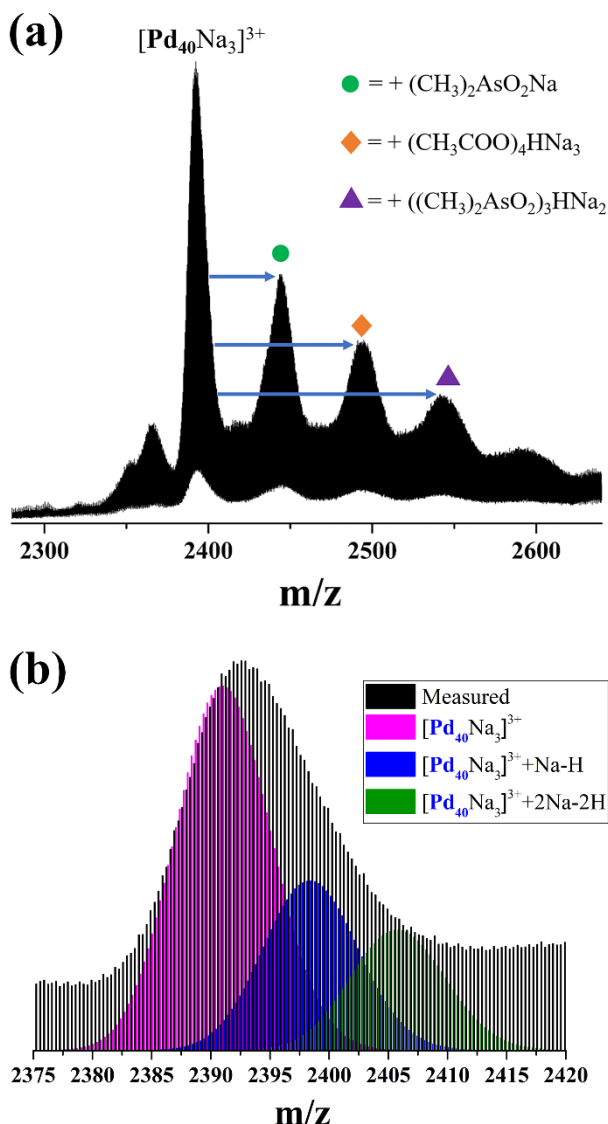


**Figure 3.** (a) ESI-MS spectrum of  $\text{Pd}_{40}\text{-SiW}_{12}$ . (b) Measured isotopic distribution of  $\text{Na}_3\text{Pd}_{40}^{3+}$  (black) overlaid with a combination of simulated isotopic distributions of intact  $\text{Pd}_{40}$  cluster unit with complete or partial re-protonation.

triply-charged and are assigned to different adducts of the discrete, neutral  $\text{Pd}_{40}$ . The leading distribution centred at  $m/z = \sim 2392$  corresponds to the molecular formula of  $\text{Na}_3[\text{Pd}_{40}\text{O}_{24}(\text{OH})_{16}\{(\text{CH}_3)_2\text{AsO}_2\}_{16}]^{3+}$  (denoted as  $\text{Na}_3\text{Pd}_{40}^{3+}$ ). In the solid-state structure of  $\text{Pd}_{40}\text{-SiW}_{12}$ , the eight  $\mu_2\text{-O}$  groups in the central core of  $\text{Pd}_{40}$  are deprotonated and associated with eight  $\text{Na}^+$  ions. However, in aqueous solution, partial or complete re-protonation of the eight central  $\mu_2\text{-O}$  groups takes place. Figure 3b shows the deviation of the measured isotopic distribution of  $\text{Na}_3\text{Pd}_{40}^{3+}$  (black) from the simulated isotopic distribution (magenta), which may be attributed to the contributions from partially de-protonated  $\text{Na}_3\text{Pd}_{40}^{3+}$  species at higher  $m/z$ . The measured distribution reproduced well with a combination of the simulated isotopic distributions of  $\text{Na}_3\text{Pd}_{40}^{3+}$  (magenta) and its one and two  $\text{Na}^+$ -resubstituted forms (blue and green, Figure 3b), respectively. Minor peaks at higher  $m/z$  were assigned to the neutral  $\text{Pd}_{40}$  cluster unit with different degrees of associated cacodylate and acetate ions present free in solution (Figure S13).

## Catalytic Studies.

The hydrogenation of arenes is an important industrial reaction primarily because (i) it provides us with a relatively simple route to useful saturated carbo- and heterocycles;<sup>22</sup> (ii) hydrogenation processes provide us with a means to cleaner fossil fuels by lowering the percentage of aromatics in diesel fuels, thereby increasing the cetane number.<sup>23</sup> Metals, especially noble metals and their nanoparticles, have been found to be extremely useful in this regard.<sup>20,22</sup> Noble metal-based nanoparticles are generally formed *via* two popular routes (i) reduction of the salts of the noble metal ions and (ii) decomposition/reduction of noble metal-based organometallic compounds followed by nucleation, growth and stabilization of the resulting nanoparticles by protecting agents, such as ligands or capping groups, ionic liquids, surfactants or solid supports in order to prevent uncontrolled aggregation of the particles.<sup>20,22b,24</sup> However, these methods do not allow us to predict or tune the nanoparticle sizes before the hydrogenation/decomposition step. Therefore, we envisioned that if we design and synthesize discrete noble metal ion-based oxo-clusters of a particular size, shape and nuclearity, uniformly load them onto stable and catalytically inert supports having high surface area, such as SBA15 (to allow for easy isolation and recyclability), and subsequently reduce them under a  $\text{H}_2$  atmosphere, we should be able to isolate supported noble metal nanoparticles with easily tunable sizes.<sup>14b</sup> The size of the deposited nanoparticle depends directly on the size of the parent discrete noble metal oxo-cluster precursor, provided the loading is uniform and low enough to prevent aggregation. Thus, we studied the efficacy of the porous silica-supported  $\text{Pd}_{40}$  cluster as a heterogeneous pre-catalyst in the hydrogenation of various substituted benzenes.<sup>14b</sup> For the catalytic studies,  $\text{Pd}_{40}\text{-SiW}_{12}$  was used as precursor and the supported pre-catalyst  $\text{Pd}_{40}\text{-SiW}_{12}@SBA15\text{-apts}$  was obtained by dissolving  $\text{Pd}_{40}\text{-SiW}_{12}$  in water and slowly adding the 3-aminopropyltriethoxysilane (apts)-modified SBA15 (SBA15-apts) to the stirred solution, which was subsequently stirred for a day (Pd-loading  $\approx 1$  wt%, see ESI). The mixture was filtered and the residue was washed multiple times with deionized water, air dried and subsequently calcined at  $250^\circ\text{C}$  for 4 hours (heating rate =  $0.5^\circ\text{C}/\text{min}$ ) in order to obtain the pre-catalyst  $\text{Pd}_{40}\text{-SiW}_{12}@SBA15\text{-apts}$  that was eventually reduced *in situ* under  $\text{H}_2$  inside the Parr reactor, thereby generating the actual catalyst for the hydrogenation of arenes. It was found that for *o*-xylene as the substrate, the reaction was complete in  $\sim 55$  mins with a  $\sim 99\%$  conversion and a *cis/trans* ratio ( $S_{c/t}$ ) of 37:63, which is expected, since *cis*-1,2-dimethylcyclohexane is less stable than *trans*-1,2-dimethylcyclohexane (Figures 4, S14 and Table S8). The *o*-xylene was chosen as a model substrate to study the efficacy of the  $\text{Pd}_{40}\text{-SiW}_{12}@SBA15\text{-apts}$  catalyst because the reaction rate for *o*-xylene was the slowest among the monocyclic arenes (*vide infra*) and because it allows to determine methyl group isomerization and demethylation – side reactions that can happen under hydrogenation conditions and form unwanted side products. The reaction of arenes with SBA15-apts alone did not show any hydrogenation activity. The effect of catalyst calcination temperatures was monitored, which showed that the reaction with *o*-xylene as the substrate is slower with the  $\text{Pd}_{40}\text{-SiW}_{12}@SBA15\text{-apts}$  pre-catalyst calcined at  $200^\circ\text{C}$  than with the catalysts calcined at  $250$  and  $300^\circ\text{C}$ , respectively (Figure S15,  $t_{\text{completion}}$  at  $200^\circ\text{C} = \sim 135$  mins,  $t_{\text{completion}}$  at  $250$  and  $300^\circ\text{C} = \sim 55$  mins). Therefore,  $250^\circ\text{C}$  was chosen as the pre-catalyst calcination temperature. A hot filtration experiment indicated

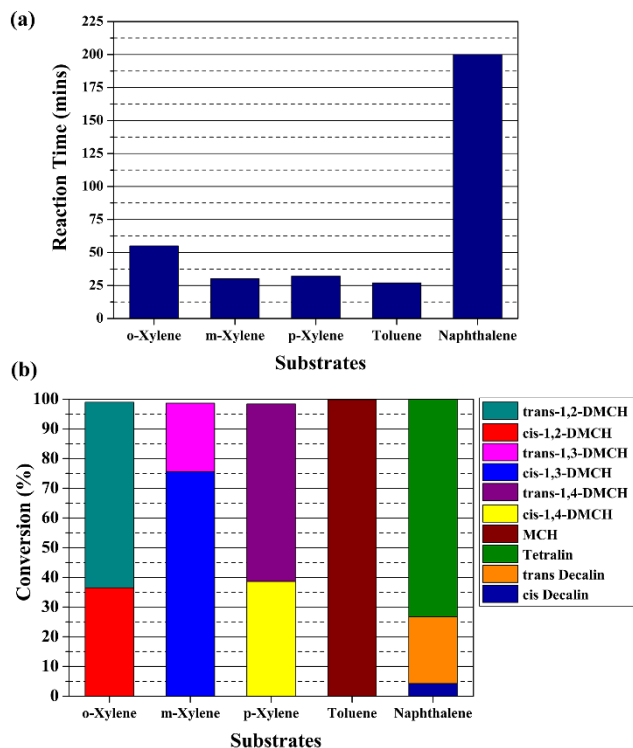


**Figure 4.** (a) Reaction times and (b) Percent conversion and selectivity for the hydrogenation of various substituted benzenes using  $\text{Pd}_{40}\text{-SiW}_{12}\text{@SBA15-apts}$  as pre-catalyst.

the heterogeneous nature of the catalytic reaction (Figure S16). The catalyst was also found to be recyclable up to 3 consecutive reaction cycles with only a marginal increase in the reaction times (Figure S17). Also,  $\text{N}_2$  sorption measurements were performed on the pre-catalyst before and after loading/calcination and after catalysis in order to investigate the effect on the surface area (Figure S18, Table S9). We found that both the surface area and pore volume of the SBA15 support decreases after modification with apts, as expected. Immobilization of  $\text{Pd}_{40}\text{-SiW}_{12}$  on the modified SBA15 further decreases the surface area and pore volume, which indicates that the pores are partially blocked upon loading, as expected. These values increase again upon calcination due to loss of the aminopropyl arms from the silica surface. After catalysis, there is a slight decrease in the surface area and pore volume, probably due to the formation of Pd nanoparticles, which are slightly larger in diameter as compared to the parent  $\text{Pd}_{40}$  oxo-cluster (*vide infra*). Elemental analysis on the freshly loaded  $\text{Pd}_{40}\text{-SiW}_{12}\text{@SBA15-apts}$  indicates a Pd:W molar ratio of  $\sim 2.4$ , which is close to the ratio of 2.2 found in the parent material  $\text{Pd}_{40}\text{-SiW}_{12}$ . Interestingly, only a negligible amount of arsenic was present, indicating that during the loading process the cacodylate groups are removed from the parent  $\text{Pd}_{40}$  cluster. This was further confirmed by measuring the  $^1\text{H}$  NMR spectrum of the filtrate obtained after loading the  $\text{Pd}_{40}\text{-SiW}_{12}$  on the modified SBA15 support, which exhibited a sharp peak at 1.6 ppm, corresponding to free Na-cac in solution (Figure S19). Incidentally, only a negligible amount of Na was observed in  $\text{Pd}_{40}\text{-SiW}_{12}\text{@SBA15-apts}$ , suggesting that the loaded  $\text{Pd}_{40}$  cluster is not associated with any  $\text{Na}^+$  ions either upon immobilization. Thus, it is likely that upon loss of the cacodylate groups, the  $\text{Pd}_{40}$  cluster is stabilized by the Keggin units and by the silica surface.<sup>25</sup> The

Pd:W molar ratios in the  $\text{Pd}_{40}\text{-SiW}_{12}\text{@SBA15-apts}$  after calcination and after catalysis were found to be  $\sim 2.5$ , which is again close to the value of  $\sim 2.2$  observed for the parent  $\text{Pd}_{40}\text{-SiW}_{12}$ . Transmission electron microscopy (TEM) analysis of the freshly loaded  $\text{Pd}_{40}\text{-SiW}_{12}\text{@SBA15-apts}$  indicates that the SBA15 is loaded with small particles (diameter ca. 1-2 nm), that are rich in Pd and W (based on TEM-EDS), see Figure S20a. The TEM analysis of  $\text{Pd}_{40}\text{-SiW}_{12}\text{@SBA15-apts}$  after calcination and catalysis indicates that the SBA15 is loaded with Pd-nanoparticles that have diameters in the range of  $\sim 2$ -6 nm, thus showing only marginal aggregation (Figures S20b). Pd nanoparticles supported on SBA15 *via* the incipient wet-impregnation method of mononuclear  $\text{Pd}^{\text{II}}$  salts have been used as hydrotreating catalysts for the upgradation of biodiesel fuels, wherein the Pd nanoparticles on the SBA-15 support were found to be in the order of 6 – 10 nm.<sup>26</sup> In addition, the Pd particle sizes in the commercial Pd/C were found to be in the order of  $\sim 12$  nm.<sup>26</sup> A point to note is that no arsenic was detected in any of the materials by TEM-EDS, which is consistent with the elemental analysis results. The TEM-Tomography analysis on the catalyst after catalysis indicates that the Pd-nanoparticles are located inside the SBA15 structure (Figure S21, see video in the ESI). We have also investigated the scope of the catalyst for heterogeneous hydrogenation by utilizing different monocyclic and bicyclic arenes as substrates (Figures 4 and S14 and Table S8). For monocyclic arenes, the reaction rate was found to be in the order *o*-xylene < *m*-xylene  $\approx$  *p*-xylene < toluene. Such an order of reactivity is consistent with the literature.<sup>27</sup> Unsaturated hydrocarbons, such as arenes, are thought to adsorb on the noble metal surface by means of a  $\pi$ -complex with a net transfer of electrons from the aromatic rings to the unoccupied *d* orbitals of the metal.<sup>27</sup> As the density of the  $\pi$ -electron cloud is higher in xylenes than in toluene (ionization potential of xylenes is higher than that of toluene) due to a larger positive inductive effect,<sup>27b</sup> the xylenes are expected to adsorb more strongly to the noble metal surface. Such high stability on the metal surface results in hydrogenation at a low rate. Among the xylene isomers, surprisingly, *o*-xylene hydrogenates at a much lower rate than *m*- and *p*-xylene, which could be attributed to a higher steric hindrance in the case of *o*-xylene.<sup>27</sup> For the bicyclic naphthalene, quantitative conversion was observed after  $\sim 200$  min with a tetralin : *cis*-decalin : *trans*-decalin ratio of 74 : 4 : 22. Such a slow reaction rate is probably due to the higher aromaticity of naphthalene as compared to the benzenes in addition to steric effects, leading to higher thermodynamic stability.<sup>27a</sup> The activity of  $\text{Pd}_{40}\text{-SiW}_{12}\text{@SBA15-apts}$  as a heterogeneous hydrogenation pre-catalyst has been compared with the industrially useful catalyst Pd/C as well as  $[\text{PdCl}_4]^{2-}$  and various polyoxopalladates (POPs) supported on SBA15-apts (Table S10).<sup>14b</sup> The activities of the various pre-catalysts were overall comparable, with the POP pre-catalysts resulting in slightly smaller nanoparticles in the range of 1-3 nm.<sup>14b</sup> However,  $\text{Pd}_{40}\text{-SiW}_{12}\text{@SBA15-apts}$  has the distinct advantage of requiring a much lower activation temperature (250 °C, as opposed to  $>550$  °C) and lower Pd-loading (Table S10).

## CONCLUSIONS

We report here on the synthesis and structure of a giant discrete and neutral disk-shaped 40-palladium(II)-oxo cluster,  $[\text{Pd}_{40}\text{O}_{56}(\text{OH})_{16}\{(\text{CH}_3)_2\text{As}\}_{16}]$  ( $\text{Pd}_{40}$ ), which is capped by 16 dimethylarsinate moieties. This is the largest neutral POC ever reported, and  $\text{Pd}_{40}$  can be isolated either as a discrete unit or as

a 3D supramolecular two-component HOIF. In the latter, **Pd**<sub>40</sub> exhibits strong H-bond interactions between its peripheral  $\mu_2$ -OH groups and the terminal oxo-groups of the Keggin ions [SiW<sub>12</sub>O<sub>40</sub>]<sup>4-</sup> or [GeW<sub>12</sub>O<sub>40</sub>]<sup>4-</sup>. Solution <sup>1</sup>H and <sup>13</sup>C NMR studies have demonstrated that **Pd**<sub>40</sub> is stable in aqueous solution (pH 7-8) for several weeks. This important fact renders **Pd**<sub>40</sub> highly interesting for biomedical studies, which are currently in progress. We have also shown that the **Pd**<sub>40</sub> cluster unit supported on a porous silica support can act as a model system for the formation of size-controlled supported Pd-nanoparticles, which are an effective heterogeneous catalyst for the hydrogenation of arenes. The discovery of the series of neutral POCs such as **Pd**<sub>16</sub>, **Pd**<sub>24</sub>, and now **Pd**<sub>40</sub> has potentially unlocked the gateway to a large family of POCs with unprecedented structures.

## ASSOCIATED CONTENT

### Supporting Information

Synthetic and catalytic procedures, instrumental details, SC-XRD refinement parameters, additional catalytic data, surface area measurements of the catalyst, additional single-crystal structural figures, PXRD, TGA and IR plots, additional NMR and ESI-MS spectra, GC spectra of the catalytic reaction solutions and TEM analysis of the catalyst. This material is available free of charge via the Internet at <http://pubs.acs.org>.

## AUTHOR INFORMATION

### Corresponding Author

**Ulrich Kortz** – Department of Life Sciences and Chemistry, Jacobs University, Campus Ring 1, 28759 Bremen, Germany;  
E-mail: [u.kortz@jacobs-university.de](mailto:u.kortz@jacobs-university.de)

### Notes

The authors declare no competing financial interest.

## ACKNOWLEDGMENT

U.K. thanks the German Research Council (DFG, KO-2288/26-1) and Jacobs University for support. X.M. thanks the China Scholarship Council (CSC) for a PhD scholarship. M.H. and E.C. thank Labex CHARMMMAT (ANR-11-LBX-0039-grant). D.T. and M.W. thank the German Research Council (DFG) for financial support for the X-ray diffraction setup (INST 1841154-1FUGG).

## REFERENCES

(1) (a) Baes, C. F.; Mesmer, R. E. *The Hydrolysis of Cations*. Krieger: 1986. (b) Wagner, A. T.; Roesky, P. W. Rare-Earth Metal Oxo/Hydroxo Clusters – Synthesis, Structures, and Applications. *Eur. J. Inorg. Chem.* **2016**, *2016* (6), 782-791.  
(2) (a) Yang, G. Y.; Huang, D. G., Chapter 9 - Cluster Compounds. In *Modern Inorganic Synthetic Chemistry (Second Edition)*, Xu, R.; Xu, Y., Eds. Elsevier: Amsterdam, 2017; pp 219-246. (b) Gross, S. Oxocluster-reinforced organic-inorganic hybrid materials: effect of transition metal oxoclusters on structural and functional properties. *J. Mater. Chem.* **2011**, *21* (40), 15853-15861. (c) Schubert, U. Surface chemistry of carboxylato-substituted metal oxo clusters – Model systems for nanoparticles. *Coord. Chem. Rev.* **2017**, *350*, 61-67. (d) Yu, Y.-Z.; Zhang, Y.-R.; Geng, C.-H.; Sun, L.; Guo, Y.; Feng, Y.-R.; Wang, Y.-X.; Zhang, X.-M. Precise and Wide-Ranged Band-Gap Tuning of Ti<sub>6</sub>-Core-Based Titanium Oxo Clusters by the Type and Number of Chromophore Ligands. *Inorg. Chem.* **2019**, *58* (24), 16785-16791. (e) Fang, W.-H.; Zhang, L.; Zhang, J. A 3.6 nm Ti<sub>52</sub>-Oxo Nanocluster with Precise Atomic Structure. *J. Am. Chem. Soc.* **2016**, *138* (24), 7480-7483. (f) Gao, M.-Y.; Zhang, L.; Zhang, J. Acid-

Controlled Synthesis of Carboxylate-Stabilized Ti<sub>44</sub>-Oxo Clusters: Scaling up Preparation, Exchangeable Protecting Ligands, and Photophysical Properties. *Chem. Eur. J.* **2019**, *25* (44), 10450-10455. (g) Geng, L.; Liu, C.-H.; Wang, S.-T.; Fang, W.-H.; Zhang, J. Designable Aluminum Molecular Rings: Ring Expansion and Ligand Functionalization. *Angew. Chem. Int. Ed.* **2020**, *59*, 16735-16740. (h) Gao, S. *Molecular Nanomagnets and Related Phenomena*. Springer Berlin Heidelberg: 2015.

(3) Woodruff, D. N.; Winpenny, R. E. P.; Layfield, R. A. Lanthanide Single-Molecule Magnets. *Chem. Rev.* **2013**, *113* (7), 5110-5148.

(4) Zheng, Z. *Recent Development in Clusters of Rare Earths and Actinides: Chemistry and Materials*. Springer Berlin Heidelberg: 2016.

(5) (a) Chen, R.; Yan, Z.-H.; Kong, X.-J. Recent Advances in First-Row Transition Metal Clusters for Photocatalytic Water Splitting. *ChemPhotoChem* **2020**, *4* (3), 157-167. (b) Han, Q.; Ding, Y. Recent advances in the field of light-driven water oxidation catalyzed by transition-metal substituted polyoxometalates. *Dalton Trans.* **2018**, *47* (25), 8180-8188.

(6) Fang, W.-H.; Zhang, L.; Zhang, J. Synthetic strategies, diverse structures and tuneable properties of polyoxo-titanium clusters. *Chem. Soc. Rev.* **2018**, *47* (2), 404-421.

(7) (a) Cao, R. *Advanced Structural Chemistry: Tailoring Properties of Inorganic Materials and their Applications*. Wiley: 2021. (b) Bhattacharya, S.; Ayass, W. W.; Taffa, D. H.; Schneemann, A.; Semrau, A. L.; Wannapaiboon, S.; Altmann, P. J.; Pöthig, A.; Nisar, T.; Balster, T.; Burtch, N. C.; Wagner, V.; Fischer, R. A.; Wark, M.; Kortz, U. Discovery of Polyoxo-Noble-Metalate-Based Metal-Organic Frameworks. *J. Am. Chem. Soc.* **2019**, *141* (8), 3385-3389.

(8) (a) Lin, Z.-E.; Yang, G.-Y. Oxo Boron Clusters and Their Open Frameworks. *Eur. J. Inorg. Chem.* **2011**, *2011* (26), 3857-3867. (b) Lin, Z.-E.; Yang, G.-Y. Germanate Frameworks Constructed from Oxo Germanium Cluster Building Units. *Eur. J. Inorg. Chem.* **2010**, *2010* (19), 2895-2902. (c) Falaise, C.; Kozma, K.; Nyman, M. Thorium Oxo-Clusters as Building Blocks for Open Frameworks. *Chem. Eur. J.* **2018**, *24* (53), 14226-14232. (d) Li, Z.; Lin, L.-D.; Yu, H.; Li, X.-X.; Zheng, S.-T. All-Inorganic Ionic Porous Material Based on Giant Spherical Polyoxometalates Containing Core-Shell K<sub>6</sub>@K<sub>36</sub>-Water Cage. *Angew. Chem. Int. Ed.* **2018**, *57* (48), 15777-15781. (e) Liu, J.-H.; Lin, L.-D.; Wang, G.-Q.; Li, L.-Y.; Sun, Y.-Q.; Li, X.-X.; Zheng, S.-T. All-inorganic open frameworks based on gigantic four-shell Ln@W<sub>8</sub>@Ln<sub>8</sub>@(SiW<sub>12</sub>)<sub>6</sub> clusters. *Chem. Commun.* **2020**, *56* (71), 10305-10308.

(9) (a) Pope, M.; Jeannin, Y.; Fournier, M. *Heteropoly and Isopoly Oxometalates*. Springer Berlin Heidelberg: 1983. (b) Pope, M. T.; Müller, A. Polyoxometalate Chemistry: An Old Field with New Dimensions in Several Disciplines. *Angew. Chem. Int. Ed.* **1991**, *30* (1), 34-48.

(10) (a) *Eur. J. Inorg. Chem.* **2009**, *34* (Issue dedicated to Polyoxometalates; Guest Ed.: Kortz, U.). (b) Dolbecq, A.; Dumas, E.; Mayer, C. R.; Mialane, P. Hybrid Organic-Inorganic Polyoxometalate Compounds: From Structural Diversity to Applications. *Chem. Rev.* **2010**, *110* (10), 6009-6048. (c) Mizuno, N.; Kamata, K. Catalytic oxidation of hydrocarbons with hydrogen peroxide by vanadium-based polyoxometalates. *Coord. Chem. Rev.* **2011**, *255* (19), 2358-2370. (d) Coronado, E.; Giménez-Saiz, C.; Gómez-García, C. J. Recent advances in polyoxometalate-containing molecular conductors. *Coord. Chem. Rev.* **2005**, *249* (17), 1776-1796. (e) Pope, M. T.; Müller, A. *Polyoxometalates: From Platonic Solids to Anti-Retroviral Activity*. Springer Netherlands: 2012. (f) Kortz, U.; Müller, A.; van Slageren, J.; Schnack, J.; Dalal, N. S.; Dressel, M. Polyoxometalates: Fascinating structures, unique magnetic properties. *Coord. Chem. Rev.* **2009**, *253* (19), 2315-2327. (g) Long, D.-L.; Burkholder, E.; Cronin, L. Polyoxometalate clusters, nanostructures and materials: From self assembly to designer materials and devices. *Chem. Soc. Rev.* **2007**, *36* (1), 105-121. (h) Müller, A.; Gouzerh, P. From linking of metal-oxide building blocks in a dynamic library to giant clusters with unique properties and towards adaptive chemistry. *Chem. Soc. Rev.* **2012**, *41* (22), 7431-7463.

(11) (a) Mal, S. S.; Kortz, U. The Wheel-Shaped Cu<sub>20</sub> Tungstophosphate [Cu<sub>20</sub>Cl(OH)<sub>24</sub>(H<sub>2</sub>O)<sub>12</sub>(P<sub>8</sub>W<sub>48</sub>O<sub>184</sub>)]<sup>25-</sup> Ion. *Angew. Chem. Int. Ed.* **2005**, *44* (24), 3777-3780. (b) Ismail, A. H.; Bassil, B.

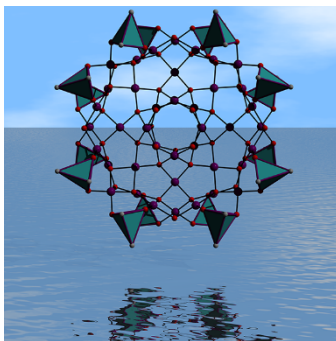
- S.; Yassin, G. H.; Keita, B.; Kortz, U.  $\{W_{48}\}$  Ring Opening: Fe<sub>16</sub>-Containing, Ln<sub>4</sub>-Stabilized 49-Tungsto-8-Phosphate Open Wheel [Fe<sub>16</sub>O<sub>2</sub>(OH)<sub>23</sub>(H<sub>2</sub>O)<sub>9</sub>(P<sub>8</sub>W<sub>49</sub>O<sub>189</sub>)Ln<sub>4</sub>(H<sub>2</sub>O)<sub>20</sub>]<sup>11-</sup>. *Chem. Eur. J.* **2012**, *18* (20), 6163-6166. (c) Yang, P.; Alsfuyani, M.; Emwas, A.-H.; Chen, C.; Khashab, N. M. Lewis Acid Guests in a  $\{P_8W_{48}\}$  Archetypal Polyoxotungstate Host: Enhanced Proton Conductivity via Metal-Oxo Cluster within Cluster Assemblies. *Angew. Chem.* **2018**, *130* (40), 13230-13235. (d) Boyd, T.; Mitchell, S. G.; Gabb, D.; Long, D.-L.; Song, Y.-F.; Cronin, L. POMzites: A Family of Zeolitic Polyoxometalate Frameworks from a Minimal Building Block Library. *J. Am. Chem. Soc.* **2017**, *139* (16), 5930-5938. (e) Uchida, S.; Mizuno, N. Design and syntheses of nano-structured ionic crystals with selective sorption properties. *Coord. Chem. Rev.* **2007**, *251* (21), 2537-2546.
- (12) (a) Döbereiner, J. W. *Journal für Chemie und Physik* **1828**, *54*, 412-426. (b) Goloboy, J. C.; Klempner, W. G. Are Particulate Noble-Metal Catalysts Metals, Metal Oxides, or Something In-Between? *Angew. Chem. Int. Ed.* **2009**, *48* (20), 3562-3564.
- (13) (a) Pley, M.; Wickleder, M. S. The Cluster Ion [Pt<sub>12</sub>O<sub>8</sub>(SO<sub>4</sub>)<sub>12</sub>]<sup>4-</sup>. *Angew. Chem. Int. Ed.* **2004**, *43* (32), 4168-4170. (b) Yang, P.; Kortz, U. Discovery and Evolution of Polyoxopalladates. *Acc. Chem. Res.* **2018**, *51* (7), 1599-1608. (c) Chubarova, E. V.; Dickman, M. H.; Keita, B.; Nadjo, L.; Miserque, F.; Mifsud, M.; Arends, I. W. C. E.; Kortz, U. Self-Assembly of a Heteropolyoxopalladate Nanocube: [Pd<sup>II</sup><sub>13</sub>As<sup>V</sup><sub>8</sub>O<sub>34</sub>(OH)<sub>6</sub>]<sup>8-</sup>. *Angew. Chem. Int. Ed.* **2008**, *47* (49), 9542-9546. (d) Barsukova, M.; Izarova, N. V.; Biboum, R. N.; Keita, B.; Nadjo, L.; Ramachandran, V.; Dalal, N. S.; Antonova, N. S.; Carbó, J. J.; Poblet, J. M.; Kortz, U. Polyoxopalladates Encapsulating Yttrium and Lanthanide Ions, [X<sup>III</sup>Pd<sup>II</sup><sub>12</sub>(AsPh)<sub>8</sub>O<sub>32</sub>]<sup>2-</sup> (X=Y, Pr, Nd, Sm, Eu, Gd, Tb, Dy, Ho, Er, Tm, Yb, Lu). *Chem. Eur. J.* **2010**, *16* (30), 9076-9085. (e) Yang, P.; Xiang, Y.; Lin, Z.; Bassil, B. S.; Cao, J.; Fan, L.; Fan, Y.; Li, M.-X.; Jiménez-Lozano, P.; Carbó, J. J.; Poblet, J. M.; Kortz, U. Alkaline Earth Guests in Polyoxopalladate Chemistry: From Nanocube to Nanostar via an Open-Shell Structure. *Angew. Chem. Int. Ed.* **2014**, *53* (44), 11974-11978. (f) Izarova, N. V.; Vankova, N.; Banerjee, A.; Jameson, G. B.; Heine, T.; Schinle, F.; Hampe, O.; Kortz, U. A Noble-Metalate Bowl: The Polyoxo-6-vanado(V)-7-palladate(II) [Pd<sub>7</sub>V<sub>6</sub>O<sub>24</sub>(OH)<sub>2</sub>]<sup>6-</sup>. *Angew. Chem. Int. Ed.* **2010**, *49* (42), 7807-7811. (g) Barsukova-Stuckart, M.; Izarova, N. V.; Jameson, G. B.; Ramachandran, V.; Wang, Z.; van Tol, J.; Dalal, N. S.; Ngo Biboum, R.; Keita, B.; Nadjo, L.; Kortz, U. Synthesis and Characterization of the Dicopper(II)-Containing 22-Palladate(II)[Cu<sup>II</sup><sub>2</sub>Pd<sup>II</sup><sub>22</sub>PV<sub>12</sub>O<sub>60</sub>(OH)<sub>8</sub>]<sup>20-</sup>. *Angew. Chem. Int. Ed.* **2011**, *50* (11), 2639-2642. (h) Xu, F.; Miras, H. N.; Scullion, R. A.; Long, D.-L.; Thiel, J.; Cronin, L. Correlating the magic numbers of inorganic nanomolecular assemblies with a {Pd<sub>84</sub>} molecular-ring Rosetta Stone. *Proc. Natl. Acad. Sci.* **2012**, *109* (29), 11609.
- (14) (a) Izarova, N. V.; Biboum, R. N.; Keita, B.; Mifsud, M.; Arends, I. W. C. E.; Jameson, G. B.; Kortz, U. Self-assembly of star-shaped heteropoly-15-palladate(II). *Dalton Trans.* **2009**, (43), 9385-9387. (b) Ayass, W. W.; Miñambres, J. F.; Yang, P.; Ma, T.; Lin, Z.; Meyer, R.; Jaensch, H.; Bons, A.-J.; Kortz, U. Discrete Polyoxopalladates as Molecular Precursors for Supported Palladium Metal Nanoparticles as Hydrogenation Catalysts. *Inorg. Chem.* **2019**, *58* (9), 5576-5582.
- (15) (a) Izarova, N. V.; Vankova, N.; Heine, T.; Biboum, R. N.; Keita, B.; Nadjo, L.; Kortz, U. Polyoxometalates Made of Gold: The Polyoxoaurate [Au<sup>III</sup><sub>4</sub>As<sup>V</sup><sub>4</sub>O<sub>20</sub>]<sup>8-</sup>. *Angew. Chem. Int. Ed.* **2010**, *49* (10), 1886-1889. (b) Xiang, Y.; Izarova, N. V.; Schinle, F.; Hampe, O.; Keita, B.; Kortz, U. The selenite-capped polyoxo-4-aurate(III), [Au<sup>III</sup><sub>4</sub>O<sub>4</sub>(Se<sup>IV</sup>O<sub>3</sub>)<sub>4</sub>]<sup>4-</sup>. *Chem. Commun.* **2012**, *48* (79), 9849-9851. (c) Izarova, N. V.; Kondinski, A.; Vankova, N.; Heine, T.; Jäger, P.; Schinle, F.; Hampe, O.; Kortz, U. The Mixed Gold-Palladium Polyoxo-Noble-Metalate [NaAu<sup>III</sup><sub>4</sub>Pd<sup>II</sup><sub>8</sub>O<sub>8</sub>(AsO<sub>4</sub>)<sub>8</sub>]<sup>11-</sup>. *Chem. Eur. J.* **2014**, *20* (28), 8556-8560.
- (16) Yang, P.; Xiang, Y.; Lin, Z.; Lang, Z.; Jiménez-Lozano, P.; Carbó, J. J.; Poblet, J. M.; Fan, L.; Hu, C.; Kortz, U. Discrete Silver(I)-Palladium(II)-Oxo Nanoclusters, {Ag<sub>4</sub>Pd<sub>13</sub>} and {Ag<sub>5</sub>Pd<sub>15</sub>}, and the Role of Metal-Metal Bonding Induced by Cation Confinement. *Angew. Chem. Int. Ed.* **2016**, *55* (51), 15766-15770.
- (17) (a) Wang, Z.; Yang, F.-L.; Yang, Y.; Liu, Q.-Y.; Sun, D. Hierarchical multi-shell 66-nuclei silver nanoclusters trapping subvalent Ag<sub>6</sub> kernels. *Chem. Commun.* **2019**, *55* (69), 10296-10299. (b) Yang, Y.; Jia, T.; Han, Y.-Z.; Nan, Z.-A.; Yuan, S.-F.; Yang, F.-L.; Sun, D. An All-Alkynyl Protected 74-Nuclei Silver(I)-Copper(I)-Oxo Nanocluster: Oxo-Induced Hierarchical Bimetal Aggregation and Anisotropic Surface Ligand Orientation. *Angew. Chem.* **2019**, *131* (35), 12408-12413. (c) Pei, X.-L.; Yang, Y.; Lei, Z.; Chang, S.-S.; Guan, Z.-J.; Wan, X.-K.; Wen, T.-B.; Wang, Q.-M. Highly Active Gold(I)-Silver(I) Oxo Cluster Activating sp<sup>3</sup> C-H Bonds of Methyl Ketones under Mild Conditions. *J. Am. Chem. Soc.* **2015**, *137* (16), 5520-5525. (d) Wong, E. L.-M.; Sun, R. W.-Y.; Chung, N. P. Y.; Lin, C.-L. S.; Zhu, N.; Che, C.-M. A Mixed-Valent Ruthenium-Oxo Oxalato Cluster Na<sub>7</sub>[Ru<sub>4</sub>(μ<sub>3</sub>-O)<sub>4</sub>(C<sub>2</sub>O<sub>4</sub>)<sub>6</sub>] with Potent Anti-HIV Activities. *J. Am. Chem. Soc.* **2006**, *128* (15), 4938-4939. (e) Chen, S.; Fang, W.-H.; Zhang, L.; Zhang, J. Atomically Precise Multimetallic Semiconductive Nanoclusters with Optical Limiting Effects. *Angew. Chem. Int. Ed.* **2018**, *57* (35), 11252-11256. (f) Toma, H. E.; Araki, K.; Alexiou, A. D. P.; Nikolaou, S.; Dovidauskas, S. Monomeric and extended oxo-centered triruthenium clusters. *Coord. Chem. Rev.* **2001**, *219-221*, 187-234. (g) Houston, J. R.; Olmstead, M. M.; Casey, W. H. Substituent Effects in Five Oxo-Centered Trinuclear Rhodium(III) Clusters. *Inorg. Chem.* **2006**, *45* (19), 7799-7805. (h) Ibrahim, M.; Dickman, M. H.; Suchopar, A.; Kortz, U. Large Cation-Anion Materials Based on Trinuclear Ruthenium(III) Salts of Keggin and Wells-Dawson Anions Having Water-Filled Channels. *Inorg. Chem.* **2009**, *48* (4), 1649-1654.
- (18) Upadhyay, A.; Rajpurohit, J.; Kumar Singh, M.; Dubey, R.; Kumar Srivastava, A.; Kumar, A.; Rajaraman, G.; Shanmugam, M. Hydroxo-Bridged Dimers of Oxo-Centered Ruthenium(III) Triangle: Synthesis and Spectroscopic and Theoretical Investigations. *Chem. Eur. J.* **2014**, *20* (20), 6061-6070.
- (19) Bhattacharya, S.; Basu, U.; Haouas, M.; Su, P.; Espenship, M. F.; Wang, F.; Solé-Daura, A.; Taffa, D. H.; Wark, M.; Poblet, J. M.; Laskin, J.; Cadot, E.; Kortz, U. Discovery and Supramolecular Interactions of Neutral Palladium-Oxo Clusters Pd<sub>16</sub> and Pd<sub>24</sub>. *Angew. Chem. Int. Ed.* **2021**, *60* (7), 3632-3639.
- (20) Tao, F.; Spivey, J. *Metal Nanoparticles for Catalysis*, RSC Catalysis Series, 2014.
- (21) (a) Atencio, R.; Briceño, A.; Galindo, X. A mesoporous hydrogen-bonded organic-inorganic framework bearing the isopolymolybdate [Mo<sub>36</sub>O<sub>112</sub>(OH)<sub>2</sub>]<sub>16</sub><sup>8-</sup>. *Chem. Commun.* **2005**, (5), 637-639. (b) Zeng, C.-H.; Luo, Z.; Yao, J. Porous hydrogen-bonded organic-inorganic frameworks: weak interactions and selective dye filtration. *CrystEngComm* **2017**, *19* (4), 613-617. (c) Aakeröy, C. B.; Beatty, A. M.; Leinen, D. S. A Versatile Route to Porous Solids: Organic-Inorganic Hybrid Materials Assembled through Hydrogen Bonds. *Angew. Chem. Int. Ed.* **1999**, *38* (12), 1815-1819.
- (22) (a) Wiesenfeldt, M. P.; Nairoukh, Z.; Dalton, T.; Glorius, F. Selective Arene Hydrogenation for Direct Access to Saturated Carbo- and Heterocycles. *Angew. Chem. Int. Ed.* **2019**, *58* (31), 10460-10476. (b) Copéret, C.; Chaudret, B.; Basset, J. M. *Surface and Interfacial Organometallic Chemistry and Catalysis*. Springer: 2005.
- (23) (a) Bader, J. M.; Rowlands, G. *Hydrocarbon Proc.* **2012**, *91*, 41-45 (b) Zhou, Z.; Zeng, T.; Cheng, Z.; Yuan, W. Preparation of a Catalyst for Selective Hydrogenation of Pyrolysis Gasoline. *Ind. Eng. Chem. Res.* **2010**, *49* (21), 11112-11118.
- (24) (a) Finke, R. G. *Metal Nanoparticles: Synthesis, Characterization and Applications*, Chap. 2. Marcel Dekker, New York, **2002**, 17-54; (b) Bradley, J. S. *Clusters and Colloids: From Theory to Application*, VCH, New York, **1994**, 459-536.
- (25) (a) Lin, Y.; Finke, R. G. Novel Polyoxoanion- and Bu<sub>4</sub>N<sup>+</sup>-Stabilized, Isolable, and Redissolvable, 20-30-ANG. Ir300-900 Nanoclusters: The Kinetically Controlled Synthesis, Characterization, and Mechanism of Formation of Organic Solvent-Soluble, Reproducible Size, and Reproducible Catalytic Activity Metal Nanoclusters. *J. Am. Chem. Soc.* **1994**, *116* (18), 8335-8353. (b) Finke, R. G.; Özkaz, S. Molecular insights for how preferred oxoanions bind to and stabilize transition-metal nanoclusters: a tridentate, C<sub>3</sub> symmetry, lattice size-matching binding model. *Coord. Chem. Rev.* **2004**, *248* (1), 135-146. (c) De Bruyn, M.; Neumann, R. Stabilization of Palladium Nanoparticles by Polyoxometalates Appended with

Alkylthiol Tethers and their Use as Binary Catalysts for Liquid Phase Aerobic Oxydehydrogenation. *Adv. Synth. Catal.* **2007**, *349* (10), 1624-1628. (d) D'Souza, L.; Noeske, M.; Richards, R. M.; Kortz, U. Palladium (0) metal clusters: Novel Krebs type polyoxoanions stabilized, extremely active hydrogenation catalyst. *Appl. Catal. A* **2013**, *453*, 262-271. (e) Villanneau, R.; Roucoux, A.; Beaunier, P.; Brouri, D.; Proust, A. Simple procedure for vacant POM-stabilized palladium (0) nanoparticles in water: structural and dispersive effects of lacunary polyoxometalates. *RSC Advances* **2014**, *4* (50), 26491-26498.

(26) Chen, S.-Y.; Chang, A.; Rungsi, A. N.; Attanatho, L.; Chang, C.-L.; Pan, J.-H.; Suemanotham, A.; Mochizuki, T.; Takagi, H.; Yang, C.-M.; Luengnaruemitchai, A.; Chou, H.-H. Superficial Pd nanoparticles supported on carbonaceous SBA-15 as efficient hydrotreating catalyst for upgrading biodiesel fuel. *Appl. Catal. A* **2020**, *602*, 117707.

(27) (a) Stanislaus, A.; Cooper, B. H. Aromatic Hydrogenation Catalysis: A Review. *Catalysis Reviews* **1994**, *36* (1), 75-123. (b) Rahaman, M. V.; Vannice, M. A. The hydrogenation of toluene and o-, m-, and p-xylene over palladium. I. Kinetic behavior and o-xylene isomerization. **1991**, *127*, 251-266. (c) Keane, M. A.; Patterson, P. M. The Role of Hydrogen Partial Pressure in the Gas-Phase Hydrogenation of Aromatics over Supported Nickel. *Ind. Eng. Chem. Res.* **1999**, *38* (4), 1295-1305.

## For Table of Contents Only



The neutral disk-shaped palladium-oxo cluster (POC)  $[\text{Pd}_{40}\text{O}_{24}(\text{OH})_{16}\{(\text{CH}_3)_2\text{AsO}_2\}_{16}]$  ( $\text{Pd}_{40}$ ) has been synthesized and structurally characterized in the solid state, in solution and in the gas phase. The novel compound  $\text{Pd}_{40}$  comprises a 40-palladium-oxo core that is capped by 16 dimethylarsinate moieties, resulting in a discrete POC with a diameter of  $\sim 2$  nm.  $\text{Pd}_{40}$  immobilized on mesoporous SBA15 support is an effective heterogeneous hydrogenation catalyst for the transformation of various arenes to saturated carbocycles.